Geophys. J. Int. (1999) **136,** 757–770

A pseudo-Thellier relative palaeointensity record, and rock magnetic and geochemical parameters in relation to climate during the last 276 kyr in the Azores region

P. P. Kruiver,[1] Y. S. Kok,[1] M. J. Dekkers,[1] C. G. Langereis[1] and C. Laj[2]

[1] *Utrecht University, Faculty of Earth Sciences, Palaeomagnetic Laboratory 'Fort Hoofddijk', Budapestlaan* 17, 3584 *CD Utrecht, the Netherlands*
[2] *Laboratoire des Sciences du Climat et de l'Environnement (LSCE), Campus du CNRS, Avenue de la Terrasse,* 91198 *Gif-sur-Yvette, France*

Accepted 1998 November 16. Received 1998 August 17; in original form 1998 January 12

SUMMARY

In the pseudo-Thellier method for relative palaeointensity determinations (Tauxe *et al.* 1995) the slope of the NRM intensity left after AF demagnetization versus ARM intensity gained at the same peak field is used as a palaeointensity measure. We tested this method on a marine core from the Azores, spanning the last 276 kyr. We compared the pseudo-Thellier palaeointensity record with the conventional record obtained earlier by Lehman *et al.* (1996), who normalized NRM by SIRM. The two records show similar features: intensity lows with deviating palaeomagnetic directions at 40–45 ka and at 180–190 ka. The first interval is associated with the Laschamps excursion, while the 180–190 ka low represents the Iceland Basin excursion (Channell *et al.* 1997). The pseudo-Thellier method, in combination with a jackknife resampling scheme, provides error estimates on the palaeointensity.

Spectral analysis of the rock magnetic parameters and the palaeointensity estimates shows orbitally forced periods, particularly 23 kyr for climatic precession. This suggests that palaeointensity is still slightly contaminated by climate. Fuzzy *c*-means cluster analysis of rock magnetic and geochemical parameters yields a seven-cluster model of predominantly calcareous clusters and detrital clusters. The clusters show a strong correlation with climate, for example samples from detrital clusters predominantly appear during rapid warming. Although both the pseudo-Thellier palaeointensity m_a and fuzzy clusters show climatic influences, we have not been able to find an unambiguous connection between the clusters and m_a.

Key words: climate, fuzzy cluster analysis, pseudo-Thellier, relative palaeointensity, rock magnetism.

1 INTRODUCTION

A knowledge of geomagnetic intensity variations is crucial to the understanding of the geodynamo. In addition, the geomagnetic field strength is believed to modulate the ^{10}Be and ^{14}C production by shielding cosmic rays and thus influencing ages obtained by ^{14}C dating (for example Raisbeck *et al.* 1987; Bard *et al.* 1990; Mazaud *et al.* 1991; Robinson *et al.* 1995). Many efforts have been made to recover the palaeointensity from sedimentary records. Principally, sedimentary sequences offer continuous high-resolution records of the natural remanent magnetization (NRM). The NRM contains information about the geomagnetic field at or shortly after the time of deposition of the sediment. However, the processes by which the sediments acquire their NRM are still not known in sufficient detail. The conventional method of extracting geomagnetic field information from the NRM signal is by performing a normalization of the NRM intensities by some normalizer. This normalizer should account for changes in magnetic grain size and concentration, which also affect the strength of the NRM signal. Different normalizers have been proposed such as saturation isothermal remanent magnetization (SIRM), anhysteretic remanent magnetization (ARM) and magnetic susceptibility κ (see Tauxe 1993). The palaeointensity would be represented by for example NRM_{25mT}/ARM_{25mT}. Similarity between normalized records obtained by different normalizers, and dissimilarity between normalized and non-normalized records are often believed to express the reliability of the palaeointensity record. Normalizing the record is assumed to minimize the effects of magnetic grain-size distribution and variation of magnetic input, for example determined by climate. Criteria for choosing the magnetic material used in palaeointensity estimates from

sedimentary sequences are summarized by Tauxe (1993). It is only possible to obtain a *relative* palaeointensity estimate from sediments in this way, in contrast to the *absolute* palaeointensity determinations from lavas and igneous rocks.

Many palaeointensity records have been published recently (e.g. Meynadier *et al.* 1992; Valet & Meynadier 1993; Weeks *et al.* 1995; Channell *et al.* 1997). Each study argues that their records represent the true geomagnetic field intensity and are free of environmental influences. It is recognized, however, that the sedimentary palaeointensity record might still be biased by environmentally caused variations in magnetic grain size and concentration (e.g. Schwartz *et al.* 1996). Although the criteria summarized by Tauxe (1993) are strict, one must be aware that there might still be some climate influence left in the normalized NRM record and that we might not be looking at a purely geomagnetic signal.

Recently, two new methods have been proposed to recover palaeointensity from sediments: the pseudo-Thellier method, based on AF demagnetization and ARM (or IRM) acquisition (Tauxe *et al.* 1995), and a Thellier–Thellier method for sediments, based on thermal demagnetization of the NRM and acquisition of a partial thermoremanent magnetization (pTRM) (Hartl & Tauxe 1996). It has been argued that these new methods diminish the environmental contamination of the palaeointensity signal better than the conventional normalizing methods. The pseudo-Thellier and the conventional method gave significantly different results for samples from the Ongtong-Java Plateau (Tauxe *et al.* 1995), whereas similar results were obtained for samples from Hole 851C (Pacific Ocean) and core MD90–0940 (Indian Ocean) by Valet & Meynadier (1998). Here, we compare the pseudo-Thellier method with ARM and the conventional normalizing method on a core spanning the last 276 kyr which seemed to have an excellent conventional palaeointensity record (Lehman *et al.* 1996). The aim of this paper is to investigate whether the pseudo-Thellier method yields different results for this core. It is important to perform such a check on a core which is likely to have suffered little diagenetic alteration. Lehman *et al.* (1996) studied several marine sedimentary cores from the Azores area, using the method of normalizing NRM by SIRM and ARM and continuous U-channel measurements. They concluded that the cores were very suitable for palaeointensity determination. In this study, we determine the palaeointensity from one of these cores (SU92–18, spanning the last 276 kyr) with the pseudo-Thellier method and with the conventional method, both on discrete samples. In addition, whole-rock geochemical analyses are carried out to study the environmental influences on the sediments in this core. Finally, fuzzy *c*-means cluster analysis on rock magnetic and geochemical parameters is performed. It provides a method of studying the relationships between rock magnetic parameters and the geochemical environment (Dekkers *et al.* 1994).

2 MATERIALS AND METHODS

The core investigated in this study is core SU92–18 from the Azores area (37°47′3″N, 27°13′9″W), north Atlantic Ocean. It is 9.93 m long and was taken from a water depth of 2300 m. The lithology seems rather homogeneous and is dominated by nannofossil ooze with clay minerals and volcanic products. A tephra layer is situated between 582 and 605 cm depth (Lehman *et al.* 1996). The average sedimentation rate was 3.5 cm kyr^{-1} based on dating by Lehman *et al.* (1996) using the $\delta^{18}O$ record from the same core, which was correlated to the oxygen isotopic record of Martinson *et al.* (1987).

Individual samples were taken by inserting 8 cm^3 perspex cylinders in the core at approximately 5 cm intervals for κ measurements and at 10 cm intervals for NRM and ARM measurements, corresponding to average resolutions of 1450 and 2900 yr, respectively. Sample numbers correspond to depths (in cm) in the core.

The magnetic susceptibility was measured with a low-field magnetic susceptibility bridge KLY2 instrument. NRM and ARM were measured with a vertical 2G RF SQUID cryogenic magnetometer (noise level 10^{-11} Am^2) in a magnetically shielded room or with a horizontal 2G DC SQUID cryogenic magnetometer (noise level 3×10^{-12} Am^2). IRM was measured on a JR5 A spinner magnetometer (noise level 5×10^{-11} Am^2). Comparison with measurements on the SQUID magnetometers showed that spinning of the moist samples in the spinner magnetometer did not affect the measurements.

Palaeointensity determinations were performed according to Tauxe *et al.* (1995) with the pseudo-Thellier method using ARM on 117 samples. We use ARM and not IRM acquisition because Tauxe *et al.* (1995) showed that the plot of ARM left versus ARM gained at the same peak field is somewhat linear, whereas IRM left versus IRM gained is markedly curved. The pseudo-Thellier method is illustrated in Fig. 1. First, the NRM is demagnetized by means of alternating fields (AF) in 14 steps up to 125 mT using steps of 5–25 mT (Fig. 1a). An ARM is then imparted at the same field steps as the NRM demagnetization. ARM_{max} indicates the ARM intensity acquired at 125 mT. The bias field was 45 μT in the direction perpendicular to the axis of the coil. Initial NRM intensities typically range from 5–300 mA m^{-1} (average 52 ± 44 mA m^{-1}) and ARM_{max} intensities from 70–800 mA m^{-1} (average 198 ± 125 mA m^{-1}). The average median destructive field (MDF) for the NRM is 25 ± 4 mT. If we plot the NRM intensity left after demagnetization versus the acquired ARM intensity (at the same peak fields, Fig. 1b) we can determine the best-fit slope, m_a (where 'a' stands for ARM), with linear regression and an error estimate using a jackknife resampling procedure (Efron 1982; Kok *et al.* 1998). The jackknife resampling procedure calculates the slope through every possible combination of at least four data points, starting at fields higher than 35 mT; 90 per cent of these slope values lie between the dashed lines in Fig. 1(c), giving an upper and lower limit for m_a. We used 35 mT field steps and higher, because the NRM left at lower steps might still be suffering from a viscous overprint. The value of m_a given in Fig. 1(b) corresponds to the slope with the smallest relative error of NRM left versus ARM gained through at least four successive data points (solid line in histogram of Fig. 1c).

The determination of m_a with the pseudo-Thellier method in combination with the jackknife resampling procedure is based on a linear relationship between ARM gained and ARM left at the same field steps (Tauxe *et al.* 1995). To check this relationship, the ARM_{max} of nine samples, selected to have a wide range of initial ARM intensities, was AF demagnetized in three perpendicular directions at the same field steps as the ARM acquisition. This was done for the DC bias field perpendicular and parallel to the AF direction (Fig. 2). The relationship is not linear for the 'perpendicular' ARM: the samples are more easily demagnetized than magnetized,

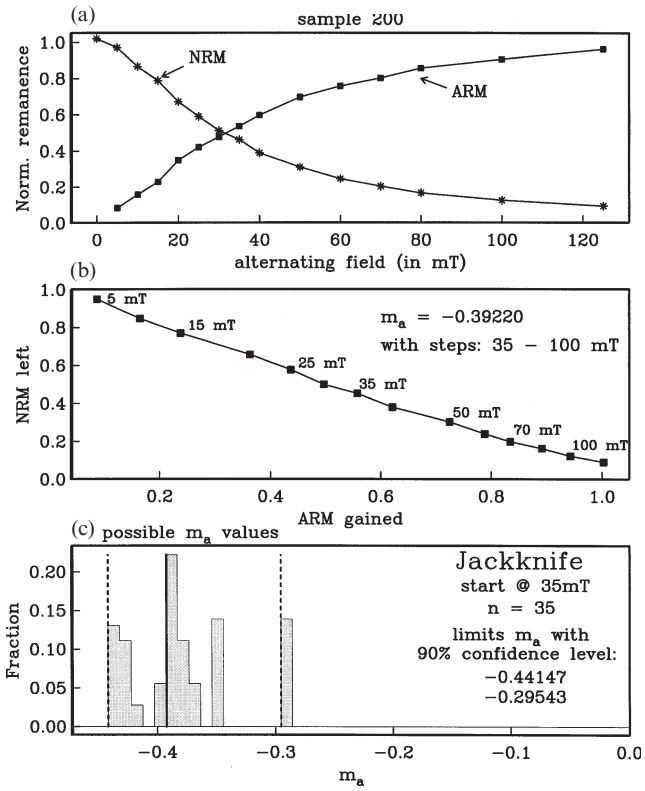

Figure 1. Pseudo-Thellier method for sample 200. (a) Stepwise AF demagnetization of NRM and (corrected) acquisition of ARM; intensities are normalized by their maximum values, initial NRM intensity is 55.5 mA m^{-1}, maximum ARM intensity is 120.5 mA m^{-1}. (b) NRM intensity left after demagnetization to a given peak field versus ARM intensity gained at the same peak field. The best-fit slope through at least four successive data points is palaeointensity estimate m_a (solid line in c); other possible values for the slope are determined with the jackknife resampling method, resulting in an upper and lower limit for m_a; (c) histogram of possible m_a values. Solid line: best-fit slope through at least four successive data points; dashed lines: upper and lower limits of 90 per cent of possible m_a values. Jackknife parameters: n is the number of calculated slopes. Determination of slopes from fields of 35 mT and higher.

particularly at higher fields (Figs 2a and b). The 'parallel' ARM shows a nearly linear relationship (Figs 2a and c). The perpendicular ARM acquisition intensities are too low compared to parallel ARM acquisition intensities. Therefore, the perpendicular ARM acquisition intensities, which were measured for all samples, are corrected to parallel ARM acquisition intensities by multiplication with a correction factor derived from the set of nine samples. These corrected ARM intensities are then used in the pseudo-Thellier palaeointensity determination.

To validate this correction, m_a was calculated for both parallel and perpendicular ARMs for the nine samples (Fig. 3). From this figure it is seen that the jackknife error for the 'perpendicular' m_a is larger. This is because the NRM left versus ARM gained plot is less linear than for the 'parallel' m_a. In addition, the parallel m_a is always slightly higher than the perpendicular m_a. The shape of the curve, however, remains unchanged and we conclude that our correction of perpendicular ARMs to parallel ARMs is valid.

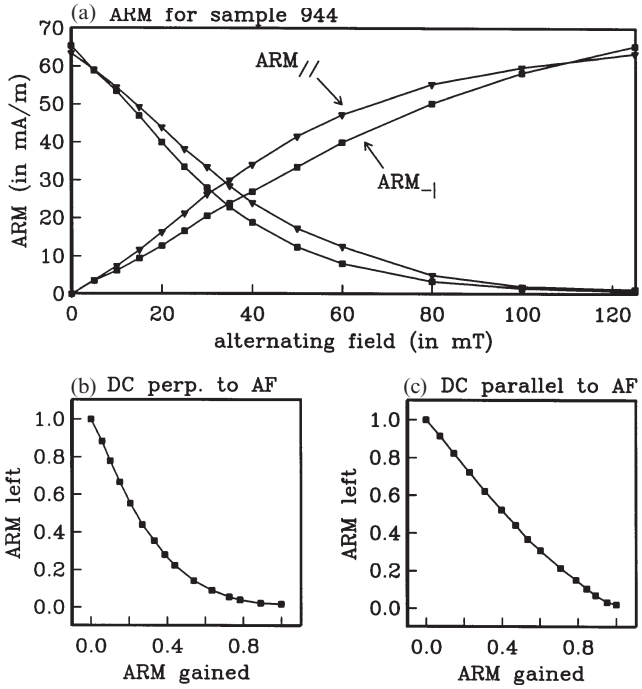

Figure 2. (a) Example of difference between 'perpendicular' and 'parallel' ARM acquisition. For parallel ARM acquisition the DC bias field was 30 μT and parallel to the AF field direction (triangles). For perpendicular ARM the DC bias field was 45 μT and perpendicular to the AF field direction (squares). Demagnetization of the ARM is also shown. (b) Average curve of nine samples of normalized ARM left after demagnetization versus ARM gained at the same field steps for perpendicular ARM acquisition. Field steps (from upper left to lower right): 0, 5, 10, 15, 20, 25, 30, 35, 40, 50, 60, 70, 80, 100 and 125 mT. Maximum ARM intensities range from 73–826 mA m^{-1}. The curve is markedly bent. (c) As (b) for parallel ARM acquisition. The curve is nearly linear. For the determination of the palaeointensity with the pseudo-Thellier method (Tauxe *et al.* 1995), the measured perpendicular ARM intensities are converted to parallel ARM intensities by multiplication with a correction factor determined from the average curves shown in (b) and (c).

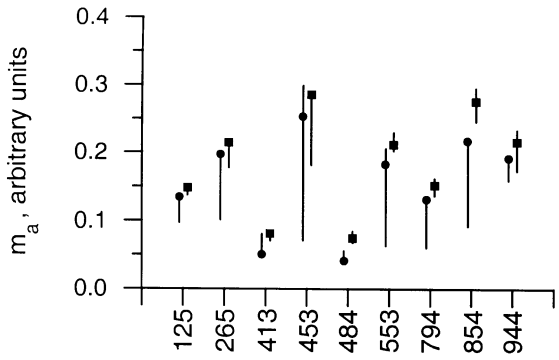

Figure 3. Comparison of palaeointensity estimates m_a obtained with perpendicular ARM acquisition (circles) and parallel ARM acquisition (squares) for nine samples (see text). Vertical lines denote jackknife errors at a 90 per cent confidence level. x-axis labels are sample numbers.

IRM acquisition with subsequent AF and DC demagnetization was performed on eight samples to screen for possible magnetic interaction (Henkel 1964; Cisowski 1981). IRM was imparted with a PM4 pulse magnetizer. Stepwise acquisition and

demagnetization were carried out up to fields of 250 mT for AF treatment and up to 800 mT for DC treatment. A three-component IRM (Lowrie 1990) was thermally demagnetized. Orthogonal IRM fields were 2.7 T, 500 mT and 80 mT. Curie balance experiments on magnetic extracts have already been performed by Lehman *et al.* (1996). In the present study, thermomagnetic runs were performed on selected samples with a modified horizontal translation Curie balance, which uses a sinusoidally cycling field instead of a steady field (Mullender *et al.* 1993). The extraction of magnetic material was not necessary for thermomagnetic analysis.

Geochemical data from 108 samples were obtained with ICP-OES analysis (inductively coupled plasma optical emission spectrometer, Perkin Elmer-type Optima 3000). The samples were dried, crushed and ground to a powder. About 250 mg of each sample was completely dissolved in a mixture of HF, HNO_3 and $HClO_4$. The samples were heated overnight, evaporated to dryness and diluted with HCl and demineralized water for analysis. Accuracy and precision were checked with laboratory standards and duplicate analyses. The analytical error was better than 5 per cent for Ca, Mn, Fe, Al, Ti, Zr, Ba and K and better than 10 per cent for S.

Multivariate classification was carried out with fuzzy *c*-means cluster analysis (Bezdek 1981). This is a partitioning method, in which *n* cases are divided into a number of clusters. The best clustering for a certain number of clusters is calculated by minimizing the distance between a sample and its cluster centre and maximizing the distance between cluster centres. The 'fuzzy' concept implies that a sample is not forced to fit into one particular cluster, but is assigned a membership to each cluster. The membership ranges from 0 (no similarity between sample and cluster) to 1 (identical). The memberships to the clusters for one sample add up to 1. A sample is called an intermediate case when the ratio of the largest but one membership to the largest membership is more than 0.6. No *a priori* information on the existence of grouping in the data set is required. A more detailed description of the algorithm of fuzzy clustering is given in Kaufman & Rousseeuw (1990). Fuzzy *c*-means clustering was applied to the following parameters: κ, ARM_{max}, ARM_{max}/κ, Ca, S, Mn, Fe/Al, Al, Ti, Zr, Ba and K. The parameters are standardized before the fuzzy cluster algorithm is run to ascertain that all parameters have equal weight. Also, parameters with log-normal distributions (κ, ARM_{max}, S, Mn, Fe/Al, Al, Ti, Ba, K) are logarithmically transformed before standardization.

3 RESULTS

3.1 Palaeomagnetic and rock magnetic results

Almost all samples show the same NRM demagnetization behaviour. Representative demagnetization diagrams show a single-component NRM, which is demagnetized towards the origin (Figs 4a and b). The NRM is often not completely removed after demagnetization at 125 mT. This implies a rather high coercivity for magnetite, which is of PSD grain size (Lehman *et al.* 1996). The coercivity of magnetite, however, can be considerably increased by low-temperature surface oxidation (van Velzen & Zijderveld 1995). Deviating demagnetization behaviour is detected in the depth interval 636–664 cm (corresponding to 180–190 ka, Figs 4c and d). These samples contain a high-coercivity component with a direction different from the 'low'-coercivity component; the latter component is removed in fields as high as 100 mT and thus can hardly be regarded as a viscous overprint.

Declinations and inclinations are shown in Fig. 5. For the deviating demagnetization behaviour interval, both high- and 'low'-coercivity components are plotted. The high-coercivity components are determined using the great-circles method (McFadden & McElhinny 1988) and they show directions comparable to the rest of the record. The 'low'-coercivity components (removed at 80–100 mT) show directions that deviate significantly. Also, in the interval around 40 ka we find deviating declinations and steep inclinations. This represents the Laschamps excursion. The trend in declination at the very top of the core is probably caused by physical rotation during coring. The difference in inclination between this study and that of Lehman *et al.* (1996) near 550–600 cm depth is likely to have been caused by the strongly magnetic tephra layer, which might disturb U-channel measurements and accompanying deconvolution.

The results of the Curie balance measurements show that the material consists predominantly of low-Ti magnetite with a Curie temperature of approximately 570 °C (Fig. 6). Upon heating to 400 °C the titanomagnetite is exsolved into pure magnetite and an end-member of ulvöspinel, resulting in a slightly stronger magnetic phase. The irreversibility of the 400 °C run is not severe, indicating a low Ti content. The Curie temperature of the exsolved magnetite is slightly lower than the Curie temperature of pure magnetite (580 °C). A low-Ti magnetite is also indicated by the unblocking temperatures close to 580 °C of the three-component IRM (see Lowrie 1990) in Fig. 7. The Curie balance measurements agree with those of Lehman *et al.* (1996). Their rock magnetic study shows that the grain size is fairly constant throughout the whole core. The hysteresis measurements show that the grain-size range is small and that all samples fall within the pseudo-single-domain (PSD) range (Lehman *et al.* 1996). They also found a rather constant ARM_{25mT}/κ ratio, which is another indication of a mainly uniform grain size. Hence, to a first approximation, we consider variations in κ, SIRM and ARM intensities as variations in concentration. κ varies from $300–4500 \times 10^{-6}$ SI and SIRM intensities range from 12–45 Am^{-1}.

From Fig. 2(c) it is seen that even the parallel ARM acquisition and demagnetization curve used for the pseudo-Thellier palaeointensity determination is not perfectly linear. A possible explanation for this is the existence of magnetic interaction. To screen for magnetic interaction, IRM acquisition curves and corresponding DC and AF demagnetization curves were measured. The acquisition and DC demagnetization curves of IRM (Fig. 8a) show that a typical sample is saturated at approximately 250 mT. If IRM gained is plotted versus IRM left (Fig. 8b) in a so-called Henkel plot (Henkel 1964), the presence of magnetic interaction can be checked (Wohlfarth 1958). Non-linearity in the Henkel plot is usually attributed to interparticle dipolar interactions in fine-particle systems (Cisowski 1981). Our results show curves that are concave up, which suggests that some positive magnetic interaction may occur (Fearon *et al.* 1990), although this may only pertain to SD magnetite.

The results of IRM acquisition and subsequent AF demagnetization (Fig. 8c) are similar for all samples, regardless of their maximum IRM intensity values. The point of intersection of the acquisition and demagnetization curves is at

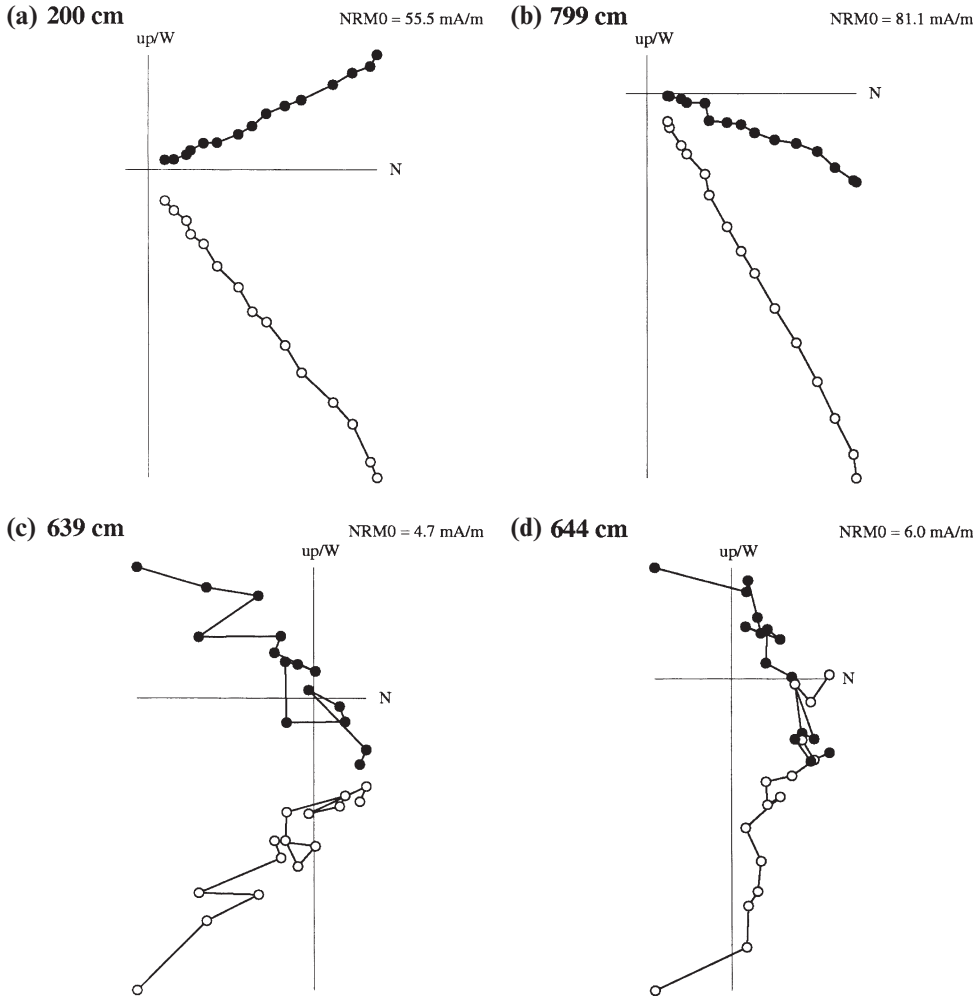

Figure 4. Zijderveld diagrams of typical samples. Solid (open) circles denote projections on the horizontal (vertical) plane. Field steps are 0, 5, 10, 15, 20, 25, 30, 35, 40, 50, 60, 70, 80, 100 and 125 mT. (a) 200 cm depth, $NRM_0 = 55.5$ mA m^{-1}; (b) 799 cm depth, $NRM_0 = 81.1$ mA m^{-1}. Zijderveld diagrams for the two-component NRM interval of depth 636–664 cm: (c) 639 cm depth, $NRM_0 = 4.7$ mA m^{-1}; (d) 644 cm depth, $NRM_0 = 6.0$ mA m^{-1}.

approximately 35 per cent of the maximum IRM intensity. Cisowski (1981) suggests that there is no magnetic interaction if the point of intersection is at 50 per cent of the maximum IRM intensity. We note, however, that Cisowski (1981) investigated magnetic interaction for SD particles and his results might not be applicable to the PSD particles in our samples.

It is unlikely, however, that magnetic interaction has played a significant role in these sediments. First, it is striking that all samples show virtually the same behaviour in these IRM experiments, independent of the absolute IRM intensities. The degree of interaction between magnetic particles is dependent on concentration (e.g. Sugiura 1979; Banerjee & Mellema 1974). If the between-grain interaction was important, samples with a relatively high concentration (i.e. high IRM intensity) and samples with a low concentration (low IRM intensity) would behave differently. All samples deviate to the same extent from the non-interaction line (slope -0.5) in the Henkel plot. Moreover, the point of intersection in the Cisowski plot (approximately 35 per cent) is the same for all samples.

Second, for magnetic interaction to occur between grains, the concentration must be much higher (>0.1–1 per cent) than is usually observed in sediments. In core SU92–18 the magnetic particles consist of (low-Ti) magnetite. Thus, magnetic interaction may occur within a particle, such as is seen in bicompositional (Housden & O'Reilly 1990; van Velzen & Zijderveld 1995) or intergrown grains (e.g. de Boer & Dekkers 1996), rather than between particles. The decrease in IRM intensity of all three induced components (Fig. 7) between 150 and 200 °C also suggests surface oxidation of the magnetic grains (van Velzen & Zijderveld 1995).

3.2 Palaeointensity estimates

Lehman *et al.* (1996) showed that the magnetic material satisfies the criteria for palaeointensity determinations of Tauxe (1993). Lehman *et al.* (1996) took NRM_{25mT}/SIRM for the conventional palaeointensity estimate. We have taken NRM_{25mT}/ARM_{max} as a conventional palaeointensity estimate because the pseudo-Thellier method uses ARM as well. Moreover, Lehman *et al.* (1996) showed that both normalizers give strikingly similar results. Both conventional palaeointensity records are shown in Fig. 9(a). In order to compare them they are both normalized by their mean values. In general, the two records agree well. The Lehman *et al.* (1996) record has a

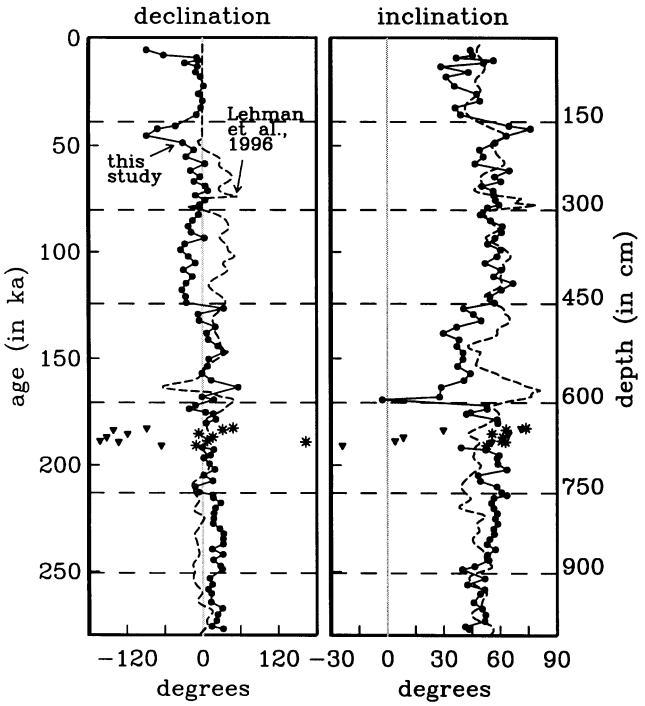

Figure 5. Declination and inclination determined from AF demagnetization. Declinations have been adjusted to obtain an average value of 0°. Dashed horizontal lines indicate core boundaries. Dashed curve is from Lehman *et al.* (1996) (continuous U-channel measurements); solid line with solid symbols (discrete samples) is from this study. Both hard (asterisks) and 'soft' (inverted triangles) components are plotted for the two-component NRM interval of 636–664 cm depth (age 180–190 ka). Hard components have been determined using great circles.

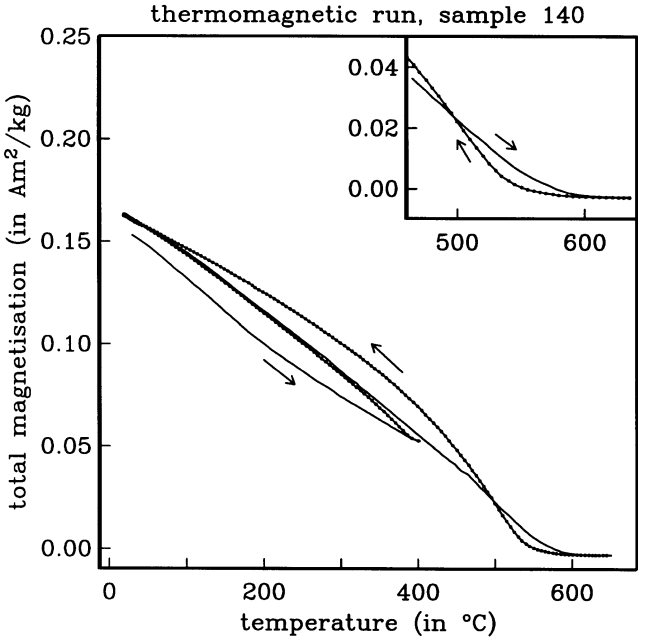

Figure 6. Thermomagnetic run of sample 140 on a modified horizontal Curie balance with a cycling field (150–300 mT). First run to 400 °C; second run to 650 °C. Method: in air; heating and cooling rate: 10° min^{-1}; mass: 26.19 mg. Sample holder correction is applied. Solid line represents heating, bold dotted line represents cooling. Curie temperature (570 °C, see inset) indicates low-Ti magnetite.

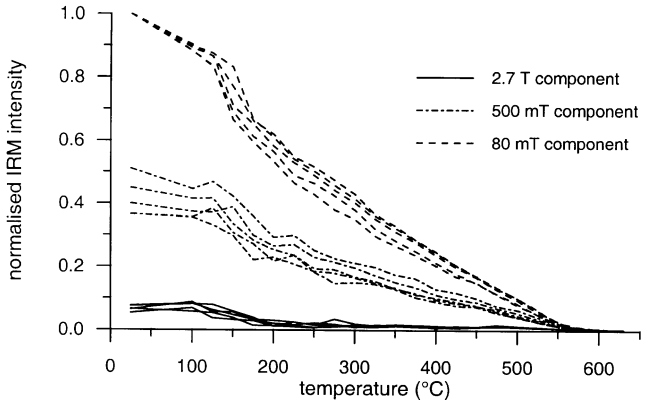

Figure 7. Thermal demagnetization of three-component IRM (Lowrie 1990). Maximum IRM fields of 2.7 T, 500 mT and 80 mT were applied subsequently along three orthogonal directions for samples 160, 408, 616, 729, 819.

higher resolution than ours, because of continuous U-channel measurements.

The pseudo-Thellier palaeointensity m_a is given in Fig. 9(b). Again the record is normalized by the mean, resulting in positive values for m_a. The solid line represents the best-fit slope found with at least four successive data points. The shaded area gives 90 per cent of all possible values of m_a according to the jackknife resampling method (see for explanation Fig. 1). Comparing the conventional record and the pseudo-Thellier record it is seen that both records show prominent intensity lows at 40–45 and 180–190 ka. From the declination and inclination plot (Fig. 5) we conclude that the 40–45 ka low corresponds to the Laschamps excursion (see Nowaczyk *et al.* 1994 and references therein). No deviating directions, however, are detected for the Blake excursion (110–120 ka). The 180–190 ka low-intensity interval corresponds to the 636–664 cm depth interval, which shows deviating NRM demagnetization behaviour, representing the Icelandic Basin reversal excursion at approximately 188 ka (Channell *et al.* 1997); this is discussed in Section 4.4. The high peak at about 170 ka is caused by a tephra layer. The values for NRM, ARM and IRM intensities of this layer are very different from the rest of the core. Therefore, we consider this peak as a lithological rather than a geomagnetic feature.

The jackknife resampling scheme applied to the pseudo-Thellier data provides an estimate of errors in the palaeointensity. This error comprises the information contained in the sample about NRM and ARM acquisition. The NRM and ARM measurements were accurate, so the experimental errors contained in the jackknife errors are insignificant. The 90 per cent confidence limit shows that the intensity determined could well have been lower or higher in some intervals compared to the conventional method.

3.3 Geochemical analyses

An overview of the average content of some geochemical elements of core SU92–18 and their standard deviations is given in Table 1. Many geochemical elements follow the same down-core pattern as the magnetic parameters, for example κ and Ti (Figs 10a and b). Ti, as well as Al and Zr, is regarded as a detrital input indicator. $CaCO_3$ (biogenic input, Fig. 10c)

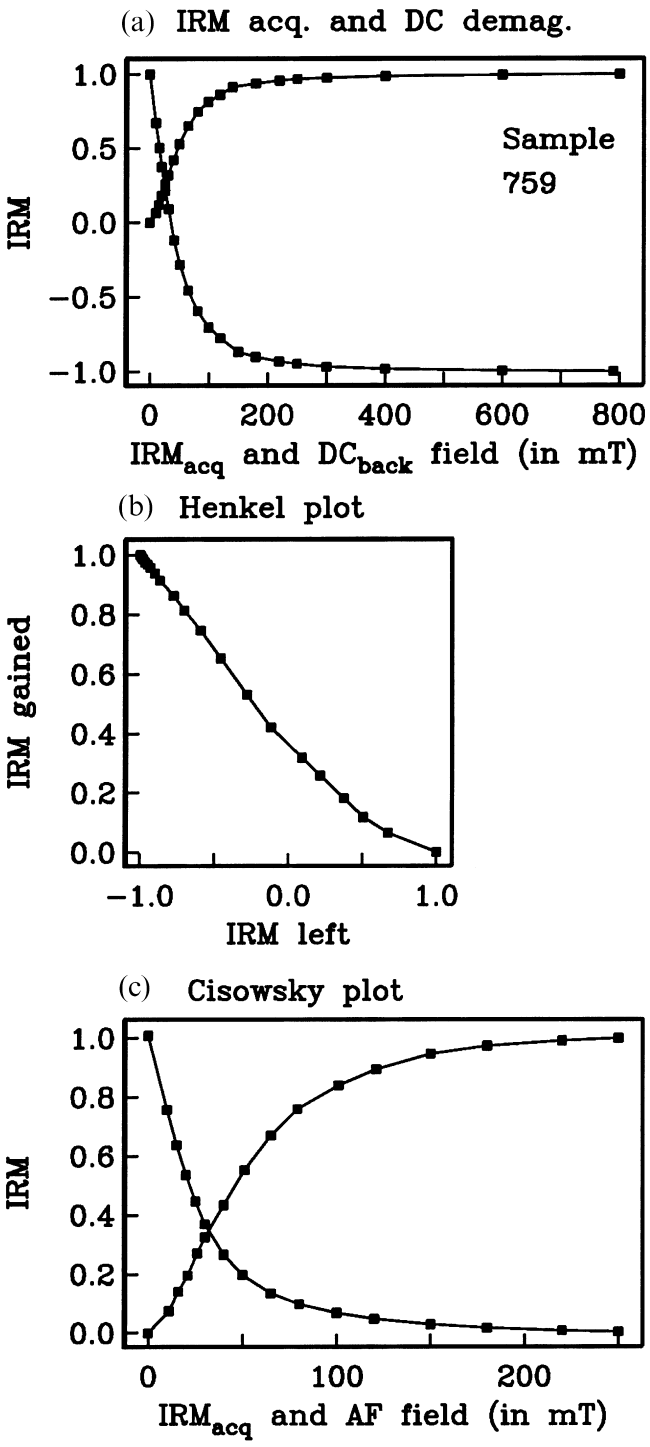

Figure 8. (a) IRM acquisition and subsequent DC demagnetization with a back field of sample 759. SIRM is 29.9 A m^{-1}. (b) Henkel plot (Henkel 1964): IRM acquired at given peak field versus IRM left at the same back field. Field steps as in (a). The absence of a linear relationship could indicate magnetic interaction. (c) Cisowski plot (Cisowski 1981): IRM acquisition and subsequent AF- demagnetization. IRM$_{250mT}$ is 28.8 A m^{-1}. The crossing point of 35 per cent, rather than 50 per cent, also indicates magnetic interaction. All intensities are normalized by their maximum values.

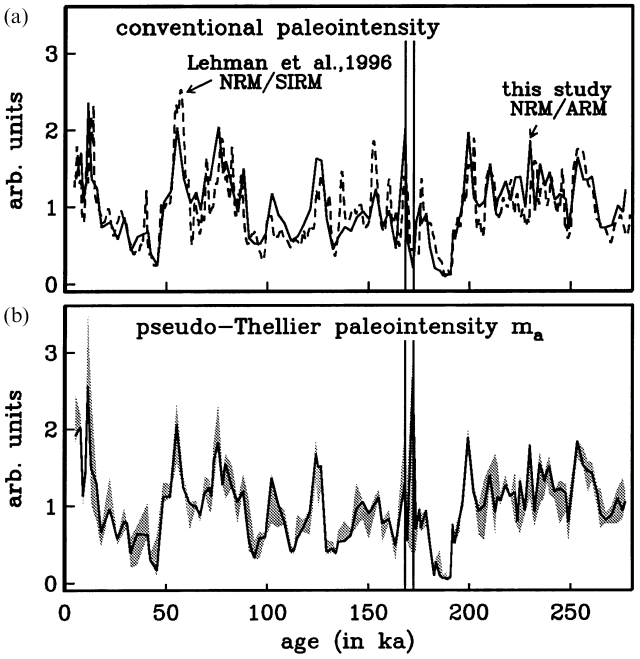

Figure 9. (a) Palaeointensity estimate using a conventional method. Dashed line is from Lehman *et al.* (1996), NRM$_{25mT}$/SIRM; solid line is from this study, NRM$_{25mT}$/ARM$_{max}$. (b) Pseudo-Thellier palaeointensity estimate m_a. Solid line is the best-fit slope m_a through at least four successive data points from the NRM left versus ARM gained plot for each sample (Fig. 1b); shaded areas indicate upper and lower limits of 90 per cent confidence level of slope m_a determined by jackknife resampling. Peaks in conventional intensity often correspond to maximum values of m_a. Both palaeointensity estimates show low-intensity intervals at 40–45 ka and 180–190 ka.

Table 1. Geochemical elements from core SU92–18 with their mean values and standard deviations. The geometric mean is given when an element is logarithmically distributed.

		Lognormal distributions		
element	unit	geometric mean, b	$b + s_L$	$b - s_L$
P	ppm	738	951	573
S	ppm	1377	1853	1024
Ni	ppm	18.2	26.8	12.3
Ba	ppm	392	521	296
Ti	%	0.40	0.61	0.26
Fe	%	2.06	3.02	1.40
Al	%	2.95	3.96	2.19
K	%	1.12	1.42	0.88

		Normal distributions	
Element	Unit	Mean	Standard deviation
Mn	ppm	643	125
Zr	ppm	177	65
Sr	ppm	1115	160
$CaCO_3$	%	59.4	9.8
Na	%	2.4	0.4

anti-correlates with κ. This suggests that the magnetic particles in the sediment have a detrital origin. Moreover, the pattern of κ calculated on a carbonate-free basis closely resembles that of κ. This indicates that the variations in κ are not a

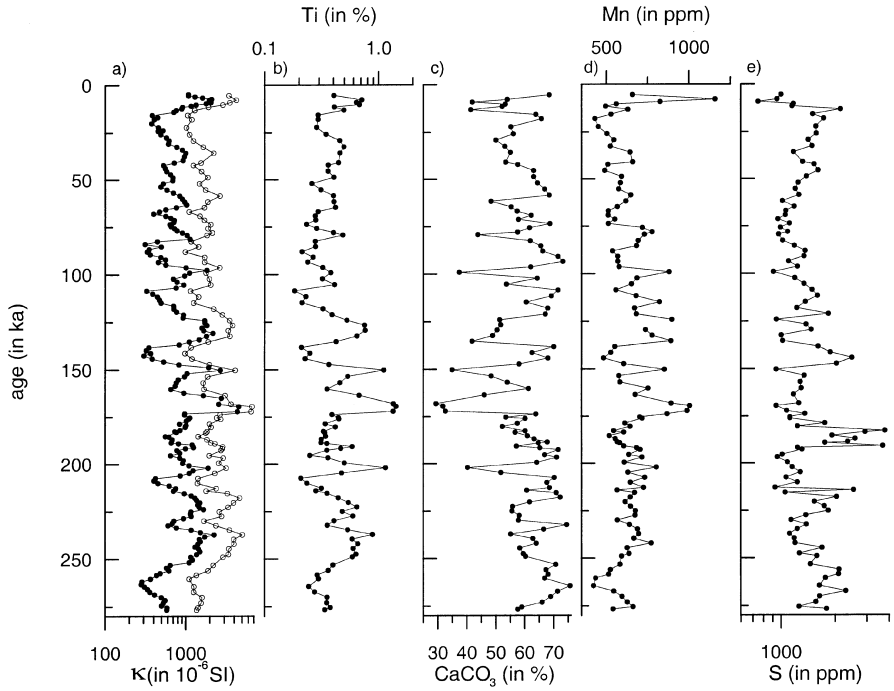

Figure 10. Geochemical results compared to κ: (a) κ (filled symbols) and κ on a carbonate-free basis (open symbols) in 10^{-6} SI; (b) Ti (per cent); (c) $CaCO_3$ (per cent); (d) Mn (ppm); (e) S (ppm). Ti and Ca show good correlations with κ, suggesting that magnetic particles are of detrital origin. Maxima in Mn correspond to maxima in Ti, indicating that diagenesis did not affect this sediment to a major extent. S shows a remarkable peak at the low-intensity two-component NRM interval of 636–664 cm depth.

result of dilution by $CaCO_3$. Similar to κ, the patterns in most parameters do not significantly change upon carbonate correction; only Al and K show a slight decrease in amplitude, whilst S variations show somewhat increased amplitudes.

Fe and Mn are indicators of palaeoredox conditions (Finney *et al.* 1988). The Fe pattern corresponds to Ti, which indicates that Fe is detrital and has not migrated as a result of diagenesis. Mn (Fig. 10d) shows a background level, with peaks corresponding to peaks in Ti. This also suggests that the effects of diagenesis on the NRM are not important in this core. S (Fig. 10e) shows a different behaviour: maxima in S correspond more or less to minima in Ti. The interval of relatively high S content corresponds to the two-component low-intensity NRM interval (636–664 cm).

3.4 Fuzzy *c*-means cluster analysis

We have applied fuzzy *c*-means cluster techniques on a number of rock magnetic and geochemical parameters. (1) Rock magnetic: κ and ARM_{max} as parameters indicative of concentration; ARM_{max}/κ as a grain size indicator; (2) geochemical: Ca and Ba as proxies for biogenic input; Al, Ti and Zr for detrital input; Fe/Al, Ba and Mn as indicators for redox potential; S indicates anoxic conditions and K is a proxy for pore-water content. NRM_{25mT} and palaeointensity estimates were not included in the cluster analysis because we aimed to assess whether the palaeointensity record would be influenced by non-magnetic parameters. In a preliminary geochemical cluster analysis, the top 130 cm of the core disturbed clustering for the rest of the core. Some samples from the top formed separate clusters with only one or two samples per cluster, while the rest of the samples from the top were intermediate cases. This suggests that in the top 130 cm transient processes may occur which complicate whole-core analysis. Therefore, in the combined geochemical/magnetic analysis we have omitted the top 130 cm.

Fuzzy *c*-means clustering was performed for two to seven clusters. Cluster centres are given in Table 2 for the two-cluster model and in Table 3 for the seven-cluster model. The most prominent features of the seven-cluster model are summarized in Fig. 11. Bivariate scatter plots of $CaCO_3$ versus Ti (Figs 12a

Table 2. Fuzzy *c*-means cluster centres for the two-cluster model. Cluster 1 is mainly detrital, cluster 2 mainly calcareous. $CaCO_3$, Al, Ti and K in per cent, ARM_{max} and ARM_{max}/κ in 10^{-6} Am^2, κ in 10^{-6} SI, S, Mn, Zr and Ba in ppm, Fe/Al dimensionless.

symbol	●	○
parameter	cluster 1	cluster 2
$CaCO_3$	51.6	65.3
ARM_{max}	2.00	1.04
ARM/κ	1587	1751
κ	1261	595
S	1271	1466
Mn	712	600
Fe/Al	0.75	0.69
Al	3.76	2.38
Ti	0.55	0.31
Zr	215	145
Ba	414	356
K	1.27	0.99

Table 3. Fuzzy *c*-means cluster centres for the seven-cluster model. Units as in Table 2. Clusters are ranked according to their $CaCO_3$ content. Clusters 1, 2 and 3 are detrital; clusters 5, 6 and 7 are calcareous. Cluster 4 is a transitional detrital/calcareous cluster.

symbol	▼	●	■	◆	▽	○	□
	detrital			transitional	calcareous		
parameter	cluster 1	cluster 2	cluster 3	cluster 4	cluster 5	cluster 6	cluster 7
$CaCO_3$	33.8	52.1	56.3	59.7	65.8	66.8	68.5
ARM_{max}	4.52	1.58	2.19	1.23	0.96	1.35	0.74
ARM/κ	1503	1608	1558	1672	1804	1650	1878
κ	3012	988	1410	726	533	819	395
S	1070	1165	1403	1699	1280	1260	1834
Mn	908	701	673	597	617	652	519
Fe/Al	1.02	0.64	0.80	0.67	0.60	0.73	0.79
Al	5.82	3.65	3.61	2.93	2.39	2.42	1.92
Ti	1.24	0.43	0.61	0.37	0.29	0.36	0.25
Zr	198	257	187	183	145	139	111
Ba	276	420	482	408	343	309	399
K	1.15	1.53	1.12	1.18	1.05	0.91	0.84

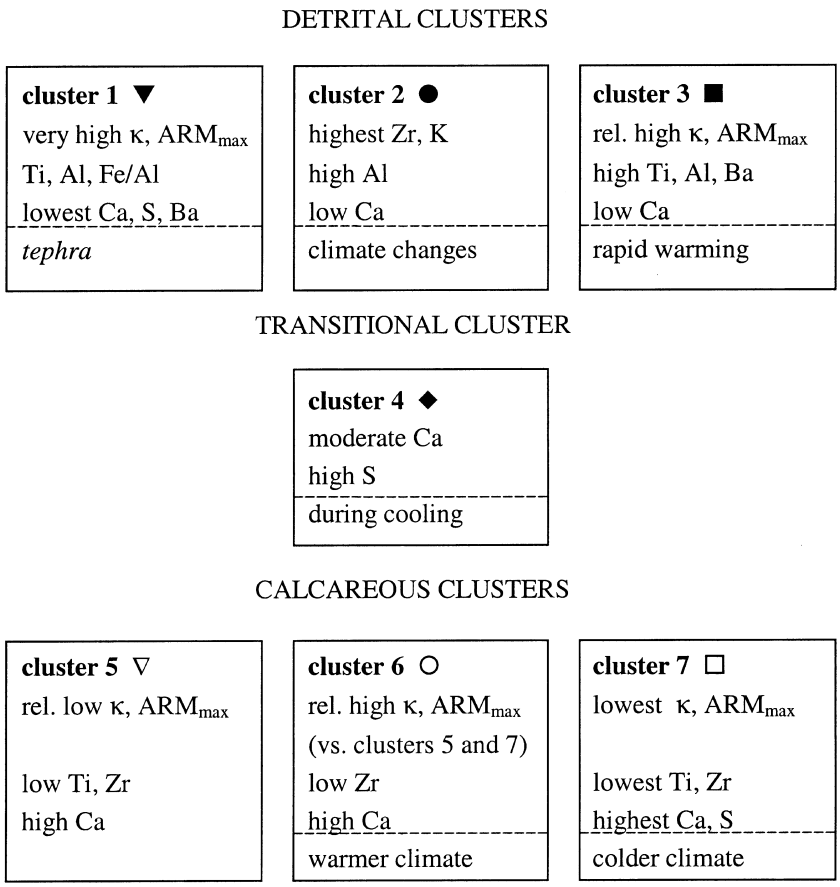

Figure 11. Schematic representation of cluster characteristics for the seven-cluster model.

and b) and Zr versus Ti (both detrital input indicators) (Figs 12c and d) illustrate the interpretation of the cluster analysis. $CaCO_3$ was calculated from Ca, assuming that 98 per cent of Ca resides in $CaCO_3$. For the two-cluster model (Fig. 12a), one cluster shows a low $CaCO_3$ and high Ti content and the other cluster a relatively high $CaCO_3$ and low Ti content. Intermediate samples fall between the two clusters. The first cluster, with high Ti, Zr and Al contents, is interpreted as a cluster with dominant detrital characteristics. The second cluster, containing more $CaCO_3$, is interpreted as a calcareous cluster with a mainly biogenic origin.

By increasing the number of clusters, a more subtle character within the detrital and calcareous clusters emerges. The detrital category is split into a tephra layer (very high Ti content, cluster 1), a detrital cluster with relatively high Ti (cluster 3) and a cluster with relatively a high Zr content (cluster 2). The calcareous category divides into a cluster with a high S content (cluster 7) and clusters with relatively high ARM_{max} and κ,

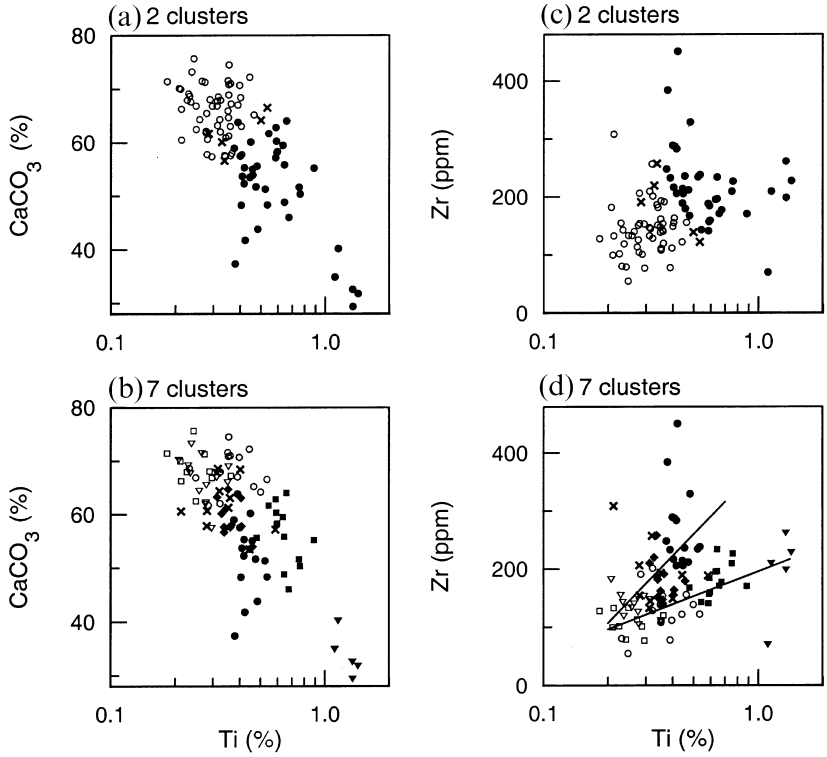

Figure 12. Bivariate cluster plots. (a) $CaCO_3$ versus Ti for two clusters: cluster 1 = detrital (filled circles), cluster 2 = calcareous (open circles), intermediate samples = crosses. (b) $CaCO_3$ versus Ti for seven clusters: cluster 1 = filled triangles; 2 = filled circles; 3 = filled squares; 4 = filled diamonds; 5 = open triangles; 6 = open circles; 7 = open squares; intermediate samples = crosses. Detrital clusters are 1, 2 and 3; calcareous clusters are 5, 6 and 7. Cluster 4 is a transitional detrital/calcareous cluster. See Fig. 11 for cluster characteristics;. (c) Zr versus Ti for two clusters, symbols as in (a). (d) Zr versus Ti for seven clusters, symbols as in (b). The two lines of clusters—1, 3, 6 and 2, 4, 5—indicate different source areas.

and low Ti within the calcareous category (clusters 6 and 5, respectively). The interval of low palaeointensity at 180–190 ka is recognized as (part of) a separate cluster (cluster 4) which has relatively high S.

In the seven-cluster model, two groups of clusters develop apart from the detrital and calcareous division. This is illustrated Fig. 12(d). One group consists of clusters 1, 3 and 6 (filled triangles, filled squares and open circles), the other group of clusters 2, 4 and 5 (filled circles, filled diamonds and open triangles). These groups of clusters lie on lines with different slopes. Moreover, inspection of the correlation matrix of all parameters considered (not shown) reveals that log(Ti) correlates highly with $\log(ARM_{max})$, log(Fe), log(Al), $\log(\kappa)$ and anti-correlates highly with Ca. Z, however, correlates highly only with log(K), correlates moderately with log(Al) and anti-correlates moderately with Ca. Thus, the detrital indicators Ti and Z show clearly different behaviour. Calculation of parameters on a carbonate-free basis (e.g. Fig. 10a) indicates that variation in the parameters is not due to dilution by $CaCO_3$. These observations point to two different source areas of detrital material: one with relatively high Ti and low Zr and the other with high Zr and low Ti.

For the seven-cluster model, the cluster assignment of each sample is plotted on the δ^{18}O-SPECMAP curve (Fig. 13). Cluster 3 samples (detrital and high κ, Ti, Al, Ba) occur during periods of rapid warming of the climate. We associate this kind of detrital sample with increased detrital input after the end of an ice age. During rapid warming (i.e. melting of the ice cover) there is still no or little vegetation in source areas. Detrital material is readily available and will be transported because of increased erosion. This results in mainly detrital samples, apparently with a relatively high Ti content. As the climate warms up, vegetation reappears and the detrital input decreases, resulting in a relatively higher calcareous content. Also, prevailing wind directions might change because of the shifting of high- and low-pressure systems, and therefore the provenance might change as well.

From the calcareous clusters, it is remarkable that cluster 6 occurs predominantly in warmer climates and cluster 7 in colder climates. During warmer periods there is increased precipitation and chemical erosion, resulting in increased run-off and a relatively more detrital calcareous cluster (cluster 6) than in colder periods (cluster 7). Cluster 2 (detrital, with highest Zr) typically occurs during (minor) changes from warming to cooling and vice versa. Cluster 4 dominates on the cooling parts of the curve. Although we see a correlation between the clusters and climate we are unable to explain all of the connections. Additional biostratigraphical and oceanographical information is probably needed for a more complete understanding of the relations.

4 DISCUSSION

4.1 Spectral analysis and correlation with climate

Changes in ice-sheet volume caused by orbital forcing are recorded in shells of for example planktonic foraminifera as fluctuations in the δ^{18}O ratio. We test for potential climate

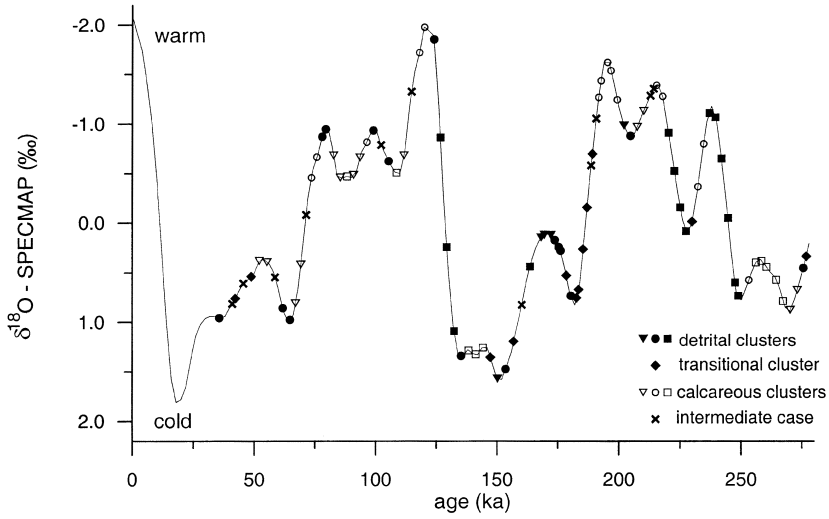

Figure 13. Seven-cluster model and δ^{18}O-SPECMAP (Imbrie *et al.* 1984). Symbols as in Fig. 12(b). Cluster 3 samples (filled squares) predominantly occur during rapid warming. Cluster 6 samples (open circles) occur during warmer climates, cluster 7 samples (open squares) during colder climates. Note that the upper 130 cm of the core was not included in the fuzzy *c*-means cluster analysis.

influence on the magnetic parameters and palaeointensity estimates of the present study by performing a spectral analysis. The spectral analysis was performed with the CLEAN algorithm of Roberts *et al.* (1987), which was developed for unequally spaced time-series. In this procedure, the 'dirty' spectra are first calculated and then 'CLEANed' by iteration. The procedure has been repeated for different window steps, gains and numbers of iterations. The CLEAN parameters which gave the most consistent spectra ($dF = 1$, gain $= 1$, 500 iterations) were chosen for all magnetic and geochemical parameters.

Frequency spectra of the parameters are checked for the presence of the Earth's orbital frequencies. All spectra are normalized by their mean values. The δ^{18}O record of SU92–18 contains the Earth's orbital periods of eccentricity (100 kyr), obliquity (41 kyr) and climatic precession (23 kyr) (Fig. 14a). Also, the spectra of magnetic parameters κ and NRM show frequencies that can be attributed to obliquity (41 kyr) and precession (23 and 19 kyr) (Fig. 14b). The ARM spectrum (not shown) is identical to that of κ. The spectrum of the NRM normalized by ARM in the conventional way (Fig. 14c) still shows spectral amplitudes at the climatic frequencies, particularly at 23 kyr^{-1}. This is also true for the pseudo-Thellier palaeointensity estimate m_a. Thus, normalizing the NRM has not removed all environmental influences.

As with the magnetic parameters, the geochemical parameters are also influenced by climate. Ba (not shown) and Ca, both regarded as palaeoproductivity indicators (e.g. Elderfield 1990) consistently show power at all climatic frequencies (Fig. 14d). Al (not shown) and Ti, representing detrital input, show peaks at obliquity and precession frequencies. S, however, seems to be influenced by obliquity and precession (19 kyr). For Ca and Ti the 19 kyr precession peak seems to be shifted to a shorter period (approximately 17 kyr).

4.2 Comments on the pseudo-Thellier method

Although palaeointensity records obtained by the conventional method and the pseudo-Thellier method do not differ considerably for this core, there is still an important advantage of performing the pseudo-Thellier method. Unlike the conventional method, the pseudo-Thellier method used in combination with a jackknife procedure provides an error estimate. Intensity information contained in the NRM signal of a whole range of (relatively higher) coercivities is included in the palaeointensity estimate, not just one single point as with the conventional method.

In the conventional ARM normalizing method, saturation of ARM is generally not tested. A standard alternating peak field is applied to each sample. This peak field might saturate different samples to a different degree, introducing an artefact in the normalization parameter. In the pseudo-Thellier method ARM saturation is not required because a number of ARM acquisition steps are used in the determination of the palaeointensity. Although not required, stepwise ARM acquisition of the pseudo-Thellier method provides a check of ARM saturation.

However, there are some pitfalls with the pseudo-Thellier palaeointensity record which appear for the conventional palaeointensity method as well. Problems arise for multicomponent NRMs. With multicomponent NRMs the slope m_a cannot be determined reliably because the intensity of the primary component is obscured by secondary components. On the other hand, the stepwise NRM demagnetization required for the pseudo-Thellier method reveals a multicomponent NRM if present.

4.3 Magnetic-grain-size estimates

The ratio ARM/κ is generally regarded as a grain-size indicator. For magnetite, this ratio varies inversely with grain size (King *et al.* 1982). However, ARM and κ respond differently to changes in grain size. Therefore, this interpretation might not be so straightforward. ARM/κ is not only sensitive to the average grain size of the magnetic particles, but also to the grain-size distribution. A relatively broader distribution with the same average particle size suffers from two effects: higher ARM, because of relatively more SD particles, and higher κ from relatively more MD particles. The resulting effect on the

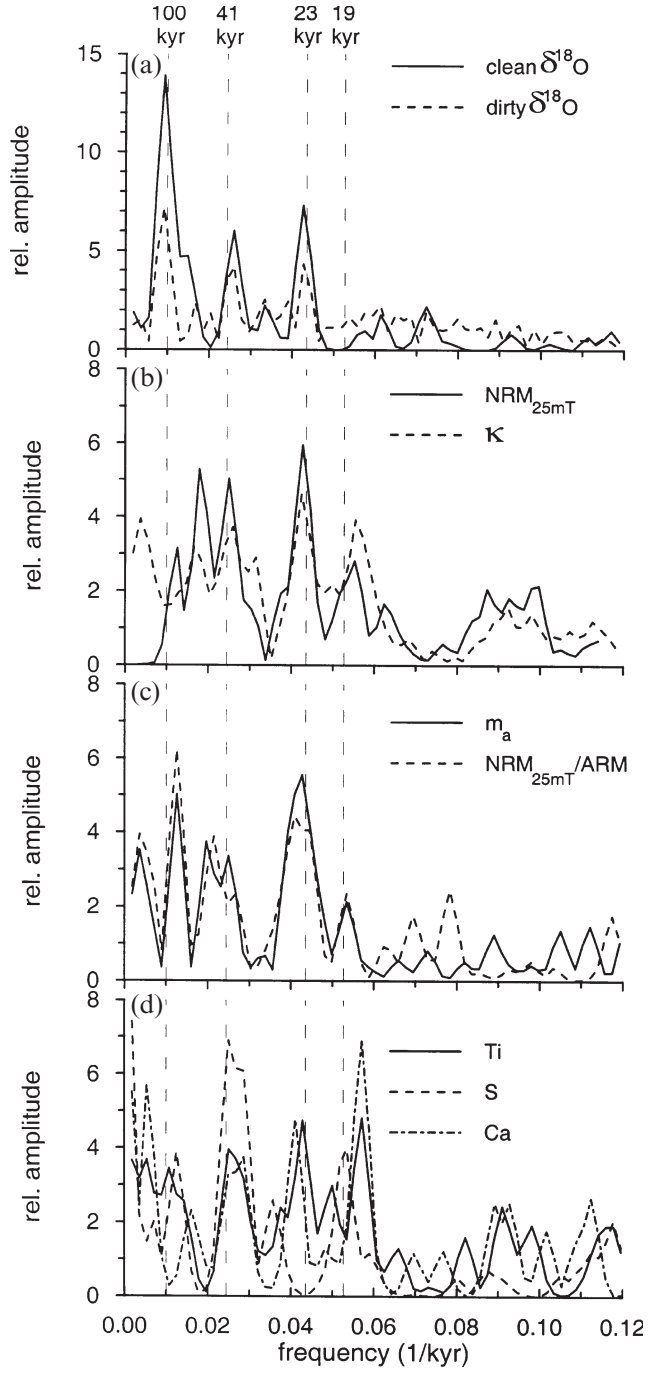

Figure 14. Spectral analysis performed with the CLEAN algorithm of Roberts *et al.* (1987). Milankovitch periods, indicated by dashed vertical lines, are 100 kyr for eccentricity, 41 kyr for obliquity and 23 and 19 kyr for climatic precession. (a) Dirty and clean frequency spectrum of δ^{18}O of SU92–18; (b) clean frequency spectra of magnetic parameters NRM_{25mT} and κ; (c) clean frequency spectra of pseudo-Thellier palaeointensity estimate m_a and conventional palaeointensity estimate NRM_{25mT}/ARM_{max}; (d) clean spectra of Ti, S and Ca. All spectra are normalized by their mean values.

ratio ARM/κ is unknown. Moreover, ARM and κ do behave differently with concentration variations. Even at low concentrations, magnetic interaction influences ARM, so the ratio ARM/κ is affected by concentration as well (Yamazaki & Ioka 1997; Sugiura 1979).

A third effect which must be considered is the clay-mineral content. This deserves special attention when κ is low and is not mainly determined by ferrimagnetic minerals. For example, chlorite has a κ value considerably higher than kaolinite. Which clay minerals dominate depends on the type of weathering and hence on climate (e.g. Chamley 1989). The ARM/κ ratio might thus be biased by varying contributions from different clay minerals. In the present case, however, ARM and κ are perfectly correlated ($r = 0.985$), so we can assume that the main part of κ is residing in ferrimagnetic material and that there is no significant paramagnetic contribution from clay minerals.

4.4 Reversal excursions and palaeointensities

The palaeointensity record and the NRM directional record (Figs 9 and 5) indicate that the sediments from this core have recorded the Laschamps excursion. The Blake excursion, however, has not been recorded even though the Blake is globally recognized (see the compilation of Nowaczyk *et al.* 1994). The non-recording of the Blake could mean either that the Blake has not occurred globally or that the sediment is not always a good recorder, at least not of directions. Neither chemical nor rock magnetic parameters indicate that this excursion was erased by diagenesis.

The low-intensity interval from 180 to 190 ka shows a 'soft' component with coercivities up to 80–100 mT. The hard component (>100 mT) clearly has a different direction from the soft component. The directions of the hard component match the directions of the remainder of the record, while the 'soft' component significantly deviates (declination -120° and shallow/negative inclination). The results could indicate that the hard components correctly recorded the magnetic signal during or shortly after deposition and the 'soft' components are overprints. However, coercivities are too high to be considered as viscous. Alternatively, the observed NRM behaviour of this interval could be an artefact of the AF demagnetization process, because the hard component does not have a stable endpoint. The most likely interpretation is that the 'soft' components show the true directions, with the hard components acquired later by the geomagnetic field existing then, for example through later low-temperature oxidation. The timing of this excursion coincides with the Icelandic Basin reversal excursion at 188 ka (Channell *et al.* 1997). A distinct intensity low at 180–190 ka is also reported in the SINT-200 stack of Guyodo & Valet (1996) and in an independent ^{10}Be-stack (Frank *et al.* 1997). It is remarkable that this two-component NRM interval contains high S values relative to the rest of the record. However, thermomagnetic analysis did not show magnetic sulphides in this interval. We do not have an explanation for the coincidence of the high S content and the low-intensity two-component NRM in this interval.

In their high-sedimentation-rate palaeointensity record from ODP Site 983 in the Iceland Basin, Channell *et al.* (1997) tied successive palaeointensity features (H: high; L: low) to the correlative oxygen isotope stages. Some features can be recognized in the Azores record, e.g. 3–2 L (~40 ka), 5–3 L (~95 ka), 8–1H (~250 ka), while others seem to show an offset in age of approximately 5 kyr. This may be explained by small uncertainties in the respective age models. There are several features, however, which are contradictory, for example their intensity low 5–5 L at approximately 125 ka compares

unfavourably with the high intensity in our record at that age, and the interval 200–250 ka also shows discrepancies. In this interval, Channell *et al.* (1997) attribute the intensity low 7–4 L to the Pringle Falls excursion (Herrero-Bervera *et al.* 1994)—which is equivalent to the Jamaica event of Ryan (1972), redated at approximately 210 ka (Langereis *et al.* 1997)—whereas we find no evidence for a clear intensity minimum; neither record shows excursional directions. Finally, in the Iceland Basin there is evidence for another excursion, in both direction (declinations) and intensity (intensity low 8–2 L) at approximately 263 ka, which correlates well with the Calabrian Ridge 0 (CR0) reversal excursion from the Mediterranean at 261 ± 3 ka (Langereis *et al.* 1997); in the Azores record we find a corresponding intensity low, but no directional evidence for this excursion.

4.5 Palaeointensity m_a and the seven-cluster model

From the spectral analysis (Fig. 14c) it is clear that the palaeointensity estimate m_a is not free from climatic influences. The question arises why we still see climate in the palaeointensity record. An attempt to answer this question is made with the combined rock magnetic/geochemical fuzzy *c*-means cluster analysis. This independent method shows climatic influence on the properties of the core as well. However, we do not see a clear relationship between the palaeointensity m_a and the seven-cluster model. The clusters are not related to particular intervals of m_a values like in the $\delta^{18}O$ record (Fig. 13), except cluster 4 with high S and low palaeointensity. We have to keep in mind, however, that this low appears in the two-component NRM interval, so palaeointensities could not be determined reliably.

5 CONCLUSIONS

The palaeointensity records show two distinct lows at 40–45 ka and 180–190 ka. The former corresponds to the Laschamps excursion; the latter represents the Icelandic Basin excursion. The Blake, Jamaica/Pringle Falls and Calabrian Ridge 0 (CR0) excursions are not recorded in these sediments, although relatively low-intensity intervals are found at $\sim$115 ka (Blake?) and $\sim$265 ka (CR0?).

The conventional and pseudo-Thellier methods for palaeointensities give similar results. Both records are contaminated by climate, as indicated by spectral analysis. However, the extent of the climate influence is difficult to quantify. The fuzzy *c*-means clustering analysis resulted in a model with mainly calcareous versus mainly detrital clusters. Samples from detrital clusters predominantly appear during rapid warming up, after the end of an ice age. The initial lack of vegetation provides an increased detrital input; when vegetation starts to develop, the sediment input becomes more calcareous. Although both the pseudo-Thellier palaeointensity m_a and fuzzy cluster analysis on rock magnetic and geochemical data show climatic influences, we have not been able to find a viable connection between the clusters and m_a.

ACKNOWLEDGMENTS

Thanks are due to Laurent Labeyrie for access to core SU92–18. Benoît Lehman is thanked for his help with sampling the core and access to his data. We acknowledge Frits Hilgen and Lisa Tauxe for their useful discussions and Cor de Boer for his help with the Curie balance measurements and interpretation. The critical and constructive comments of an anonymous reviewer greatly improved this manuscript This study is partly supported by the Netherlands Geoscience Foundation (GOA/NWO). This work was conducted under the programme of the Vening Meinesz research School of Geodynamics. A table with all relevant data can be found at the URL www.geo.uu.nl/geophysics/html/paleo/forth.html.

REFERENCES

Banerjee, S.K. & Mellema, J.P., 1974. A new method for the determination of paleointensity from the A.R.M. properties of rocks, *Earth planet. Sci. Lett.,* **23,** 177–184.

Bard, E., Hamelin, B., Fairbanks, R.G. & Zindler, A., 1990. Calibration of the ^{14}C timescale over the past 30,000 years using mass spectrometric U-Th ages from Barbados corals, *Nature,* **345,** 405–410.

Bezdek, C.J., 1981. *Pattern Recognition with Fuzzy Objective Function Algorithms,* Plenum Press, New York.

Chamley, H., 1989. *Clay Sedimentology,* Springer-Verlag, New York.

Channell, J.E.T., Hodell, D.A. & Lehman, B., 1997. Relative paleointensity and $\delta^{18}O$ at ODP Site 983 (Gradar Drift, North Atlantic) since 350 ka, *Earth planet. Sci. Lett.,* **153,** 103–118.

Cisowski, S., 1981. Interacting vs. non-interacting single domain behavior in natural and synthetic samples, *Phys. Earth planet. Inter.,* **26,** 56–62.

de Boer, C.B. & Dekkers, M.J., 1996. Grain-size dependence of the rock magnetic properties for a natural maghemite, *Geophys. Res. Lett.,* **23,** 2815–2818.

Dekkers, M.J., Langereis, C.G., Vriend, S.P., van Santvoort, P.J.M. & Lange, G.J., 1994. Fuzzy c-means cluster analysis of early diagenetic effects on natural remanent magnetisation acquisition in a 1.1 Myr piston core from the Central Mediterranean, *Phys. Earth planet. Inter.,* **85,** 155–171.

Efron, B., 1982. *The Jackknife, the Bootstrap and Other Resampling Plans.,* Society for Industrial and Applied Mathematics, Philadelphia, PA.

Elderfield, H., 1990. Tracers of ocean paleoproductivity and paleochemistry: an introduction, *Paleoceanography,* **5,** 711–717.

Fearon, M., Chantrell, R.W. & Wohlfarth, E.P., 1990. A theoretical study of interaction effects on the remanence curves of particulate dispersions, *J. Mag. Magnetic Mater.,* **86,** 197–206.

Finney, B.P., Lyle, M.W. & Heath, G.R., 1988. Sedimentation at MANOP site H (eastern equatorial Pacific) over the past 4000,000 years: climatically induced redox variations and their effects on transition metal cycling, *Paleoceanography,* **3,** 169–189.

Frank, M., Schwarz, B., Baumann, S., Kubik, P.W., Suter, M. & Mangini, A., 1997. A 200 kyr record of cosmogenic radionuclide production rate and geomagnetic field intensity from ^{10}Be in globally stacked deep-sea sediments, *Earth planet. Sci. Lett.,* **149,** 121–129.

Guyodo, Y. & Valet, J.-P., 1996. Relative variations in geomagnetic intensity from sedimentary records: the past 200,000 years, *Earth planet. Sci. Lett.,* **143,** 23–36.

Hartl, P. & Tauxe, L., 1996. A precursor to the Matuyama/Brunhes transition-field instability as recorded in pelagic sediments, *Earth planet. Sci. Lett.,* **138,** 121–135.

Henkel, O., 1964. Remanenzverhalten und Wechselwirkungen in hartmagnetischen Teilchenkollektiven, *Phys. Stat. Sol.,* **7,** 919–929.

Herrero-Bervera, E. *et al.*, 1994. Age and correlation of a paleomagnetic episode in the western United States by $^{40}Ar/^{39}Ar$ dating and tephrochronology: The Jamaica, Blake, or a new polarity episode?, *J. geophys. Res.,* **99,** 24 091–24 103.

Housden, J. & O'Reilly, W., 1990. On the intensity and stability of the natural remanent magnetization of ocean floor basalts, *Phys. Earth planet. Inter.,* **64,** 261–278.

Imbrie, J. *et al*., 1984. The orbital theory of Pleistocene climate: support from a revised chronology of the marine δ18O record, in *Milankovitch and Climate,* part 1, ed. Berger, A.L., Imbrie, J., Hays, J., Kukla, G. & Saltzman, B., pp. 269–305, D. Reidel, Dordrecht.

Kaufman, L. & Rousseeuw, P.J., 1990. *Finding Groups in Data: an Introduction to Cluster Analysis,* John Wiley, New York.

King, J.W., Banerjee, S.K., Marvin, J. & Özdemir, O., 1982. A comparison of different magnetic methods for determining the relative grain size of magnetite in natural minerals, some results for lake sediments, *Earth planet. Sci. Lett.,* **59,** 404–419.

Kok, Y.S., Tauxe, L. & Pick, T., 1998. Jackknife resampling for paleointensities of the Earth's magnetic field, *Geophys. Res. Lett.,* submitted.

Langereis, C.G., de Dekkers, M.J., Lange, G.J., Paterne, M. & van Santvoort, P.J.M., 1997. Magnetostratigraphic and astronomical calibration of the last 1.1 Myr from an eastern Mediterranean piston core and dating of short events in the Brunhes, *Geophys. J. Int.,* **129,** 75–94.

Lehman, B., Laj, C., Kissel, C., Mazaud, A., Paterne, M. & Labeyrie, L., 1996. Relative changes of the geomagnetic field intensity during the last 280 kyear from piston cores in the Açores area, *Phys. Earth planet. Inter.,* **93,** 269–284.

Lowrie, W., 1990. Identification of ferromagnetic minerals in a rock by coercivity and unblocking temperature properties, *Geophys. Res. Lett.,* **17,** 159–162.

Martinson, D.G., Pisias, N.G., Hays, J.D., Imbrie, J., Moore, T.C. & Shackleton, N.J., 1987. Age dating and the orbital theory of the ice ages: development of a high resolution 0–300 000 years stratigraphy, *Quat. Res.,* **27,** 1–29.

Mazaud, A., Laj, C., Bard, E., Arnold, M. & Tric, E., 1991. Geomagnetic field control of ^{14}C production over the last 80 ky: implications for the radiocarbon time-scale, *Geophys. Res. Lett.,* **18,** 1885–1888.

McFadden, P.L. & McElhinny, M.W., 1988. The combined analysis of remagnetization circles and direct observations in palaeomagnetism, *Earth planet. Sci. Lett.,* **87,** 161–172.

Meynadier, L., Valet, J.-P., Weeks, R., Shackleton, N.J. & Hagee, V.L., 1992. Relative geomagnetic intensity of the field during the last 140 ka, *Earth planet. Sci. Lett.,* **114,** 39–57.

Mullender, T.A.T., van Velzen, A.J. & Dekkers, M.J., 1993. Continuous drift correction and separate identification of ferrimagnetic and paramagnetic contributions in thermomagnetic runs, *Geophys. J. Int.,* **114,** 663–672.

Nowaczyk, N.R., Frederichs, T.W., Eisenhauer, A. & Gard, G., 1994. Magnetostratigraphic data from late Quaternary sediments from the Yermak Plateau, Arctic Ocean: evidence for four geomagnetic polarity events within the last 170 Ka of the Brunhes Chron, *Geophys. J. Int.,* **117,** 453–471.

Raisbeck, G.M., Yiou, F., Bourles, D., Lorius, C., Jouzel, J. & Barkov, N.I., 1987. Evidence for two intervals of enhanced ^{10}Be deposition in Antarctic ice during the last glacial period, *Nature,* **326,** 273–277.

Roberts, D.H., Lehár, J. & Dreher, J.W., 1987. Time series analysis with clean. I. derivation of a spectrum, *Astr. J.,* **93,** 968–989.

Robinson, C., Raisbeck, G.M., Yiou, F., Lehman, B. & Laj, C., 1995. The relationship between ^{10}Be and the geomagnetic field strength records in central North Atlantic sediments during the last 80 ka, *Earth planet. Sci. Lett.,* **136,** 551–557.

Ryan, W.B.F., 1972. Stratigraphy of late Quaternary sediments in the Eastern Mediterranean, in *The Mediterranean Sea: A Natural Sedimentation Laboratory,* pp. 149–169, ed. Stanley, D.J., Dowden, Hutchinson & Ross, Stroudsberg, PA.

Schwartz, M., Lund, S.P. & Johnson, T.C., 1996. Environmental factors as complicating influences in the recovery of the quantitative geomagnetic-field paleointensity estimates from sediments, *Geophys. Res. Lett.,* **23,** 2693–2696.

Sugiura, N., 1979. ARM, TRM and magnetic interactions: concentration dependence, *Earth planet. Sci. Lett.,* **42,** 451–455.

Tauxe, L., 1993. Sedimentary records of relative paleointensity of the geomagnetic field: theory and practice, *Rev. Geophys.,* **31,** 319–354.

Tauxe, L., Pick, T. & Kok, Y.S., 1995. Relative paleointensity in sediments: a pseudo-Thellier approach, *Geophys. Res. Lett.,* **22,** 2885–2888.

Valet, J.-P. & Meynadier, L., 1993. Geomagnetic field intensity and reversals during the past four million years, *Nature,* **366,** 234–238.

Valet, J.-P. & Meynadier, L., 1998. A comparison of different techniques for relative paleointensity, *Geophys. Res. Lett.,* **25,** 89–92.

van Velzen, A.J. & Zijderveld, J.D.A., 1995. Effects of weathering on single-domain magnetite in Early Pliocene marine marls, *Geophys. J. Int.,* **121,** 267–278.

Weeks, R.J., Laj, C., Endignoux, L., Mazaud, A., Labeyrie, L., Roberts, A.P., Kissel, C. & Blanchard, E., 1995. Normalised natural remanent magnetisation intensity during the last 240 000 years from piston cores from the central North Atlantic Ocean: geomagnetic field intensity or environmental signal?, *Phys. Earth planet. Inter.,* **87,** 213–229.

Wohlfarth, E.P., 1958. Relations between different modes of acquisition of the remanent magnetization of ferromagnetic particles, *J. appl. Phys.,* **29,** 595–596.

Yamazaki, T. & Ioka, N., 1997. Cautionary note on magnetic grain-size estimation using the ratio of ARM to susceptibility, *Geophys. Res. Lett.,* **24,** 751–754.